Supporting Information

Dependence of the Magnetic Resonance Signal on the Magnetic Susceptibility of Blood Studied with Models Based on Real Microvascular Networks

Xiaojun Cheng[1,2], Avery J.L. Berman[2], Jonathan R. Polimeni[2,3], Richard B. Buxton[4], Louis Gagnon[2,5], Anna Devor[2,4,6], Sava Sakadžić[2], David A. Boas[1,2]

[1]Neurophotonics Center, Department of Biomedical Engineering, Boston University, MA 02215, USA
[2]Athinoula A. Martinos Center for Biomedical Imaging, Department of Radiology, Massachusetts General Hospital, Harvard Medical School, Charlestown, Massachusetts 02129, USA
[3]Division of Health Sciences and Technology, Massachusetts Institute of Technology, Cambridge, Massachusetts, 02139, USA
[4]Department of Radiology, UC San Diego, La Jolla, California 92093, USA
[5]Department of Radiology and Nuclear Medicine, Faculty of Medicine, Laval University, Quebec, Canada, G1V 0A6
[6]Department of Neurosciences, UC San Diego, La Jolla, California 92093, USA

S1. Comparison with random cylinder model

As a control experiment, we compare results obtained from VAN modeling with the random cylinder model using the same distribution of vessel sizes as the VANs. The histogram of a total of 9871 vessel segments from six VANs is shown as in Fig. S1a. In the random cylinder model as described in the methods section, the vessel sizes are drawn from this distribution and the value of β is obtained for both the BOLD and contrast agent (CA) range of $\Delta\chi$ as shown in Fig. S1b, averaged over 20 random configurations. To further explore the relation between β and $\Delta\chi$ concentration, we shown in Fig. S1c that at a fixed field strength $B_0 = 1.5$ T, β decreases continuously with increasing $\Delta\chi$ concentration. This further confirms that it is the product $B_0 \cdot \Delta\chi$ that determines the behavior of β.

Note that the values of β obtained in Fig. S1b are not exactly the same as that in Fig 2. and Fig. 5 using VAN modeling with the real mouse vasculature. This is due to the fact that the random cylinder model ignores many features such as the bifurcations and vessel curvatures that exists in real networks. A real network also has some unique structures such as large pial vessels which are not necessarily captured in a simplified random cylinder model. However, the overall behavior of β decreases with increasing B_0 and $\Delta\chi$ concentration stays the same in both simulation methods.

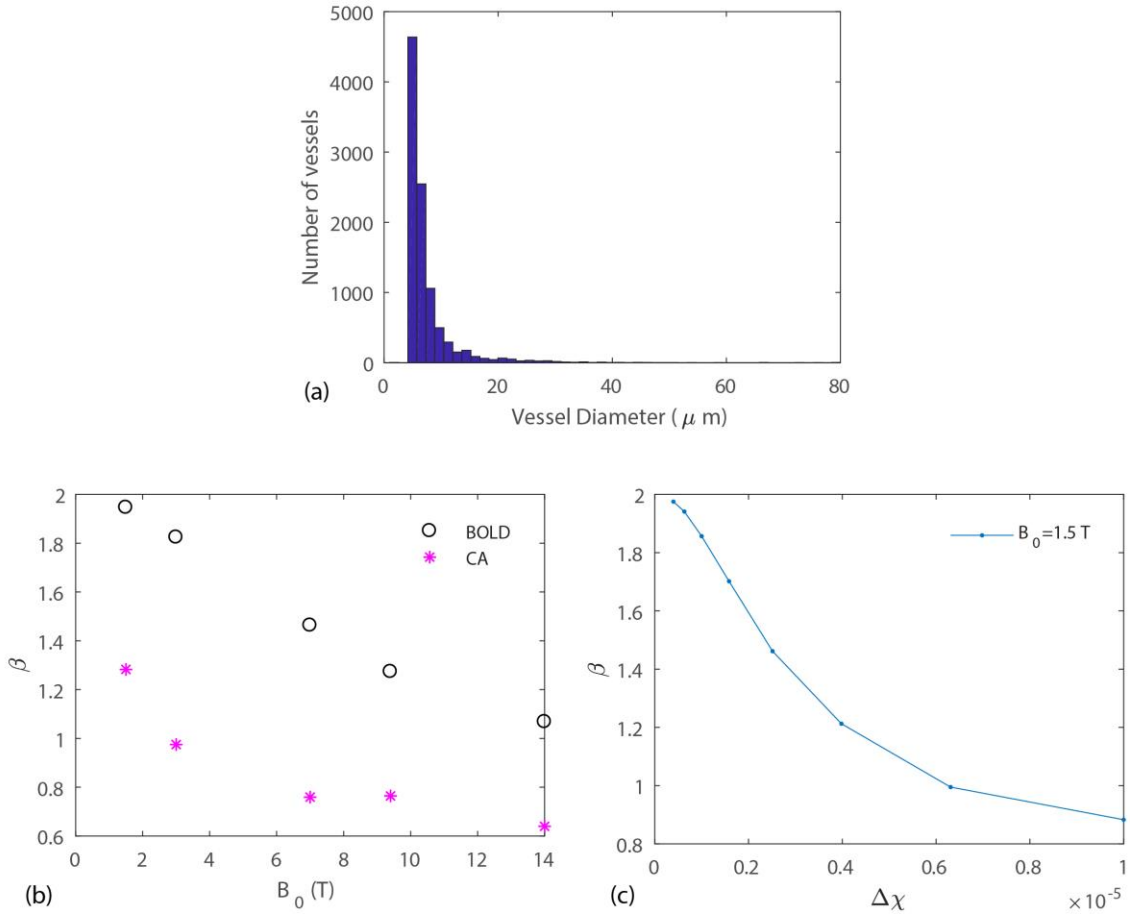

Supporting Information Figure S1. (a) The distribution of vessel sizes from the six networks of mouse vasculature measured *in vivo*. (b) β obtained from the random cylinder model with the vessel size distribution in (a) for both BOLD (2×10^{-7} to 12×10^{-7}) and CA range (1×10^{-6} to 10×10^{-6}) of $\Delta\chi$ concentration. (c) The value of β as a function of $\Delta\chi$ concentration in SI units.

S2. Oxygen distribution within a network

The oxygen distribution within the microvascular network is obtained by solving the oxygen advection-diffusion equations (1,2), and more detailed information of integrating this method in VAN modeling can be found in a previous report (3). To see the oxygen distribution within the network, the oxygen concentration in different vessel branching orders is plotted in Fig. S2b. The branching order is obtained by tracking along the vasculature starting from the pial artery and vein indicated in Fig. S2a. Vessels in branching order 7 and 8 are mostly capillaries. $\Delta\chi$ concentration and vessel diameters are shown in Fig. S2 c and d respectively. We see that $\Delta\chi$ concentration and vessel diameters are correlated and the vessels that

contain the highest $\Delta\chi$ concentration are the large veins. Thus β calculated with the deoxyhemoglobin weighted $\Delta\chi$ distribution is closer to the large vessel limit of $\beta = 1$ compared to that obtained with a uniform $\Delta\chi$ distribution.

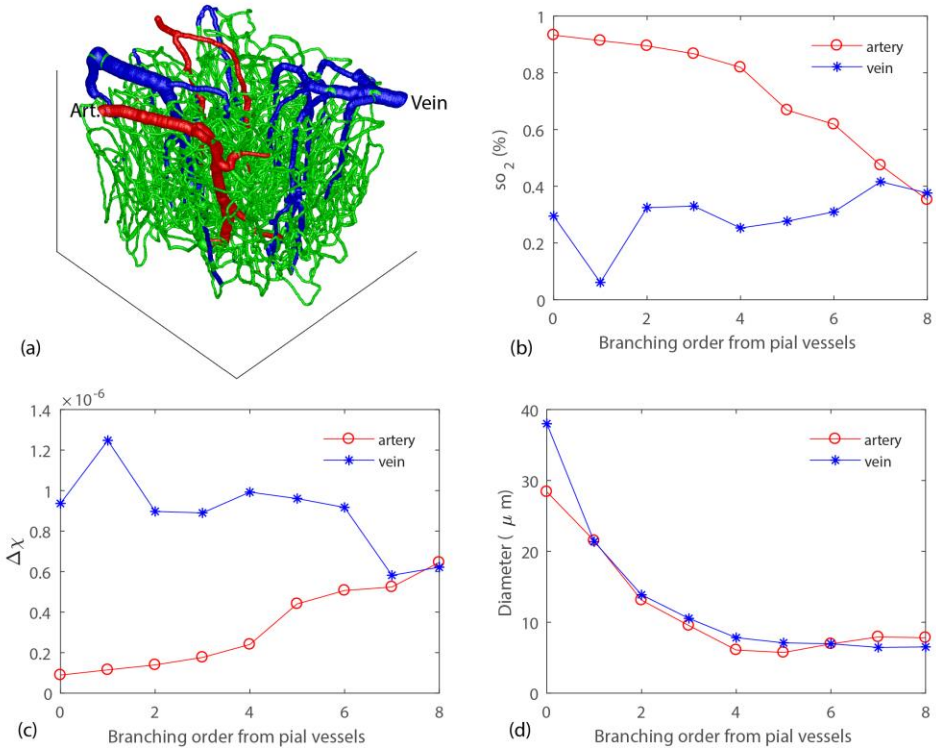

Supporting Information Figure S2. (a) The vasculature (blue: veins; red: arteries; green:capillaries) with starting pial artery and vein (branching order = 0) indicated in the figure. (b) Distribution of SO_2 computed in the model as a function of branching orders staring from the pial artery and vein. (c) $\Delta\chi$ concentration in different branching orders. (d) The corresponding vessel diameter in different branching orders.

S3. Choosing the time step in Monte-Carlo simulations

Most of the time steps used in this paper is $dt = 0.2$ ms. However, when the values of B_0 and $\Delta\chi$ are large, the typical phase accumulated within a time step $\gamma B_0 \Delta\chi\, dt$ can be larger than 2π. This raises a question of a smaller dt might be required at ultra-high magnetic field strength and large $\Delta\chi$.

To see the effect of dt on the value of β, we have calculated the value of β with different *dt*=0.1 ms for the BOLD $\Delta\chi$ range (2×10^{-7} to 12×10^{-7}) and CA range (1×10^{-6} to 10×10^{-6}) as shown in Supporting Information Figure S3. We see that at $B_0 = 9.4, 14$ T and CA range, there are noticeable differences between the values obtained at $dt = 0.1$ ms and $dt = 0.2$ ms. Further calculations are carried out at $dt = 0.05, 0.02, 0.01$ ms. The results obtained at $dt = 0.02, 0.01$ ms agree, thus, $dt = 0.01$ ms is

chosen for the values of beta in Figure 5 at $B_0 = 9.4$, 14 T, while in other cases, $dt = 0.2$ ms is sufficient. The overall behavior of β decreasing with B_0 and $\Delta\chi$ stays the same.

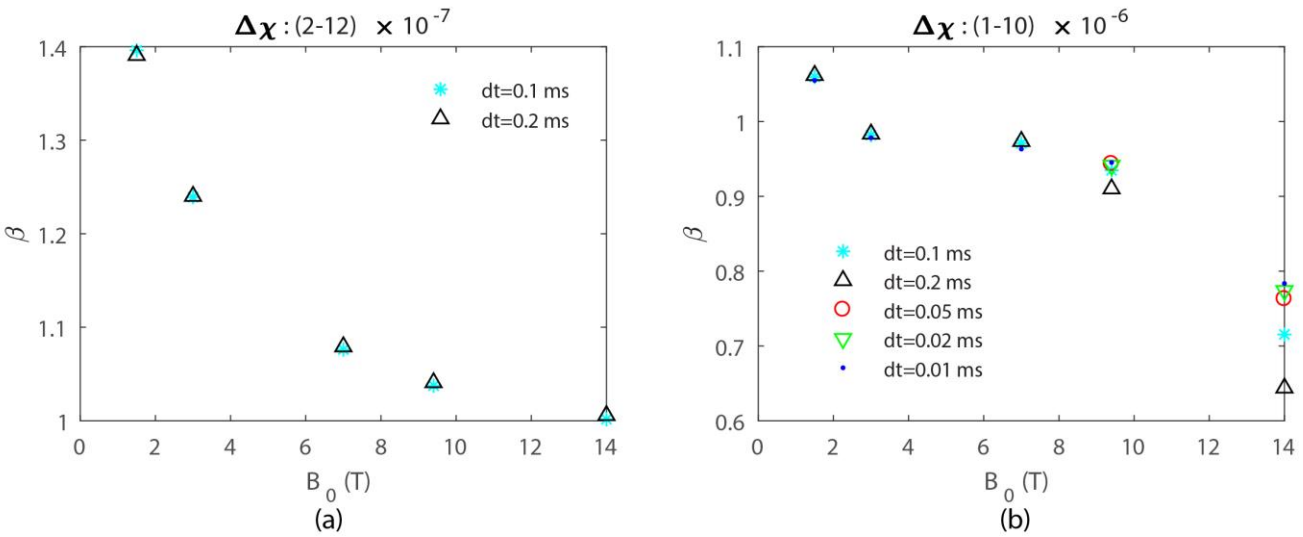

Supporting Information Figure S3. The value of β obtained for a mouse vascular for different dt values in the Monte-Carlo simulations for (a) the BOLD range of $\Delta\chi$ range (2×10^{-7} to 12×10^{-7}) and (b) contrast agent range of Δx (1×10^{-6} to 10×10^{-6}).

1. Fang Q, Sakadžić S, Ruvinskaya L, Devor A, Dale AM, Boas DA. Oxygen advection and diffusion in a three dimensional vascular anatomical network. Opt. Express 2008;16:17530.

2. Fang Q, Boas DA. Tetrahedral mesh generation from volumetric binary and grayscale images. In: 2009 IEEE International Symposium on Biomedical Imaging: From Nano to Macro. ; 2009. pp. 1142–1145. doi: 10.1109/ISBI.2009.5193259.

3. Gagnon L, Sakadžić S, Lesage F, et al. Quantifying the microvascular origin of BOLD-fMRI from first principles with two-photon microscopy and an oxygen-sensitive nanoprobe. J. Neurosci. Off. J. Soc. Neurosci. 2015;35:3663–3675. doi: 10.1523/JNEUROSCI.3555-14.2015.